SCIENTIFIC REPORTS

OPEN

SUBJECT AREAS:
ELECTROCATALYSIS
POLLUTION REMEDIATION

Received
22 January 2014

Accepted
28 March 2014

Published
23 April 2014

Correspondence and requests for materials should be addressed to S.-M.C. (smchen78@ms15.hinet.net)

Heteroatom-enriched and renewable banana-stem-derived porous carbon for the electrochemical determination of nitrite in various water samples

Rajesh Madhu, Vediyappan Veeramani & Shen-Ming Chen

Electroanalysis and Bioelectrochemistry Lab, Department of Chemical Engineering and Biotechnology, National Taipei University of Technology, No. 1, Section 3, Chung-Hsiao East Road, Taipei 106, Taiwan, ROC.

For the first time, high-surface-area (approximately 1465 $m^2 g^{-1}$), highly porous and heteroatom-enriched activated carbon (HAC) was prepared from banana stems *(Musa paradisiaca, Family: Musaceae)* at different carbonization temperatures of 700, 800 and 900°C (HAC) using a simple and eco-friendly method. The amounts of carbon, hydrogen, nitrogen and sulfur in the HAC are 61.12, 2.567, 0.4315, and 0.349%, respectively. Using X-ray diffraction (XRD), CHNS elemental analysis, X-ray photoelectron spectroscopy (XPS) and Raman spectroscopy, the prepared activated carbon appears amorphous and disordered in nature. Here, we used HAC for an electrochemical application of nitrite (NO_2^-) sensor to control the environmental pollution. In addition, HAC exhibits noteworthy performance for the highly sensitive determination of nitrite. The limit of detection (LODs) of the nitrite sensor at HAC-modified GCE is 0.07 μM. In addition, the proposed method was applied to determine nitrite in various water samples with acceptable results.

Recently, activated carbon (AC) with high specific surface area has been produced from various sources of biowaste materials because of their availability and cost effectiveness. Notably, most types of activated carbon (coal or petroleum pitch) are prone to exhaustion[1–3]. The nonuniform global distribution and the huge applications of AC widen the gap between demand and supply. The scarcity of AC may cause the AC to become expensive, which leads to the urgent need to explore carbon materials from various types of biowaste, which cost significantly less than the commercially available AC, to replace the commercial activated carbon. Interestingly, the preparation process of AC is simple, easily adopted and eco-friendly compared to the preparation of CNT and graphene. Moreover, AC has unique properties such as better electronic conductivity, surface functionality, thermal stability and high purity of the carbon content[4–11]. The high specific surface area with uniform pores allows charges and target ions to easily accumulate heteroatoms, such as H, N, B and S, on the carbon surface. Likewise, the spherical-carbon nanoparticle activated carbon (SNAC) material from mango leaves contain carbon, hydrogen, nitrogen and sulfur, whose contents are 72.6, 6.1, 6.5 and 7.46%, respectively[12]. Moreover, the AC surfaces consist of hydrophobic and hydrophilic sites; the adsorbent pore structure of the hydrophobic graphene layer and the hydrophilic surface functional groups is intricate in adsorption/desorption and catalytic applications[13].

Adsorption is a surface phenomenon that is directly related to surface area. In particular, the specific adsorption can be increased while increasing the surface area if we consider the micropores and the molecular porosity. In some cases, chemically activated carbon at a temperature of 700°C exhibits a higher adsorption of CO_2 than that at 800°C, even though the surface area of AC at 800°C is two times larger than the AC at 700°C. The AC at 700°C has a higher CO_2 adsorption because it has smaller pores than the AC at 800°C[14,15]. KOH is more effective than other alkali activating agents, and it produces carbon with notably high specific surface area from hydrothermally carbonized polysaccharides and sawdust. Moreover, the –OK groups transform into –OH groups upon KOH activation because of their ion exchange reaction. The creation of voids by removing K upon washing with water may create polar functional groups, such as –OH, which makes the carbon surface hydrophilic[16]. The prepared AC has been widely demonstrated for multiple applications such as batteries, supercapacitors, and adsorption and purification of toxic elements in the water.

We are interested in investigating the preparation of activated carbon from banana stems for electrochemical applications. Nitrite is a typical inorganic pollutant, which is highly carcinogenic to human life and aquatic animals. Moreover, nitrite is broadly used as an additive and corrosion inhibitor in food. It can produce methemoglobin, which reduces the transportation of oxygen. Furthermore, nitrite reacts with various amines and amides to form N-nitrosoamines, which cause stomach cancer[17–20]. The determination of nitrite is imperative because of their high toxicity in biological systems, particularly in children, which augments the urgent requirement to develop detection technologies. Many techniques have been developed for the in situ quantification of nitrite, including fluorescence[20], photometric methods[21], sequential injection[22], spectrophotometry[23] and electrochemical methods[24]. Among these methods, electrochemical methods are relatively cost-effective, easy to analyze, highly sensitive and highly selective[25–36]. However, AC remains as the most important factor in environmental pollution control because of its large surface area, high porous nature, high-energy adsorption sites, good electrical conductivity and electrocatalytic behavior.

As shown in Figure 1, we used a facile and eco-friendly method to derive HAC from banana stem *(Musa paradisiaca, Family: Musaceae)* for the first time to explore this material for the electrochemical nitrite sensor application. The fabricated HAC showed a high surface area of approximately 1465 m^2g^{-1}, and the contained amounts of carbon, hydrogen, nitrogen and sulfur were 61.12, 2.567, 0.4315, and 0.349%, respectively. Herein, the HAC-modified glassy carbon electrode (GCE) was modified with the AC material at different temperatures (AC700, AC800 and HAC) using various techniques. In addition, we compared the catalytic behavior of HAC towards the nitrite sensor using both DPV and the amperometric i-t method. The results revealed that the HAC-modified GCE has enormous electrochemical activity for the nitrite sensor compared with many previously reported works, as shown in Supplementary Table S1. The highly ordered porous nature of the HAC material allowed fast electron transfer due to their high-energy adsorption sites, which leads to high sensitivity and selectivity. In addition, the large surface area of HAC with micropores and mesopores enabled the highly sensitive detection of nitrite. The proposed method was also applied to determine nitrite in various water samples with acceptable results.

Results and Discussion

Figure 2a shows the typical XRD pattern of the HAC. Two broad peaks were observed at 23° and 43°, which correspond to the (002) and (100) planes, respectively. The amorphous behavior of activated carbon is revealed[37,38]. Figure 2b shows the Raman spectrum of AC at three different temperatures: AC700, AC800 and HAC. Among them, the HAC has two obvious peaks at 1311 cm^{-1} and 1580 cm^{-1}, which correspond to the D and G bands of disordered and graphitic carbons, respectively. The D and G band ratio of HAC (I_{1311}/I_{1580}) was 0.83, which indicates the amorphous carbon structure and a high content of lattice edges or plane defects of HAC[39,40]. XPS is known to analyze the chemical composition and the binding energy. Supplementary Figure S1 shows the XPS survey spectra of AC700, AC800 and HAC. HAC exhibits the peaks that correspond to carbon, oxygen, nitrogen and sulfur, which reveal the obtained results from the elemental analysis study (see Table 1). Moreover, AC700 and AC800 do not contain any binding energy peak for nitrogen, and a small peak is obtained for sulfur, which reveals the above KOH activation mechanism. Supplementary Figure S2a–d shows the enlarged regions of the XPS spectra of C1s, O1s, N1s and S2p. Figure 3a displays the XPS C1s spectrum of HAC, and the corresponding C1s peak at 285 eV reveals the high content of carbon with the assignment of the C-O bond of the C-O-R group. The small tail between 286 and 290 eV is obtained because of the C-O bond of the O-(C-O) -O group and the energy loss of the "shake-up" features. The corresponding O1s (Supplementary Figure S2b) peak at 534 eV reveals oxygen with the assignment of COH, COOH and N–O–C. Furthermore, the peak at 401.2 eV (Supplementary Figure S2c) corresponds to N atoms that are linked with three carbon atoms at the same "pyrrolic" nitrogen incorpora-

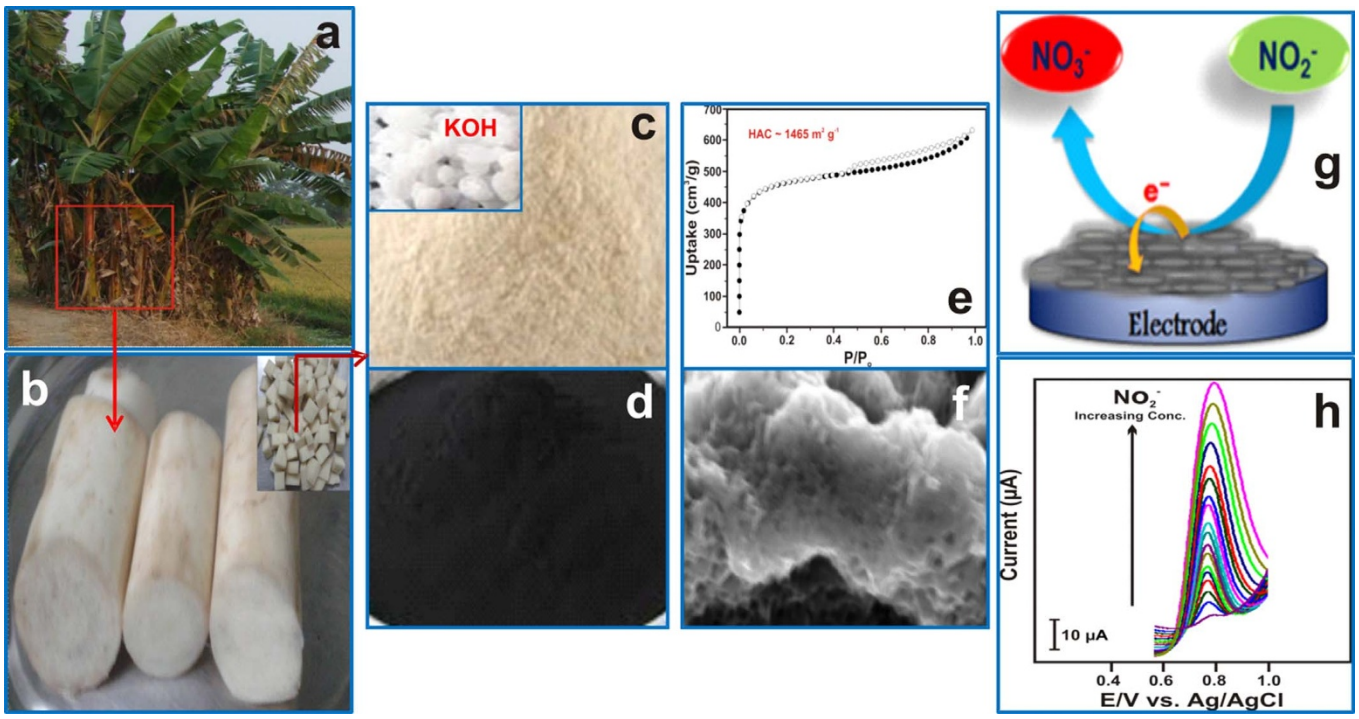

Figure 1 | A cost-effective, environmentally friendly, pollution-control and high-purity AC production from banana stem. (All photographs were taken by S.M.C and the co-authors) (a), banana tree. (b), banana stems. (c), banana stem powder. (d), HAC powder. (e), BET surface area study of HAC. (f), SEM image of porous HAC. (g), the proposed mechanism of nitrite sensor in water samples. (h), DPV catalytic behavior of nitrite oxidation.

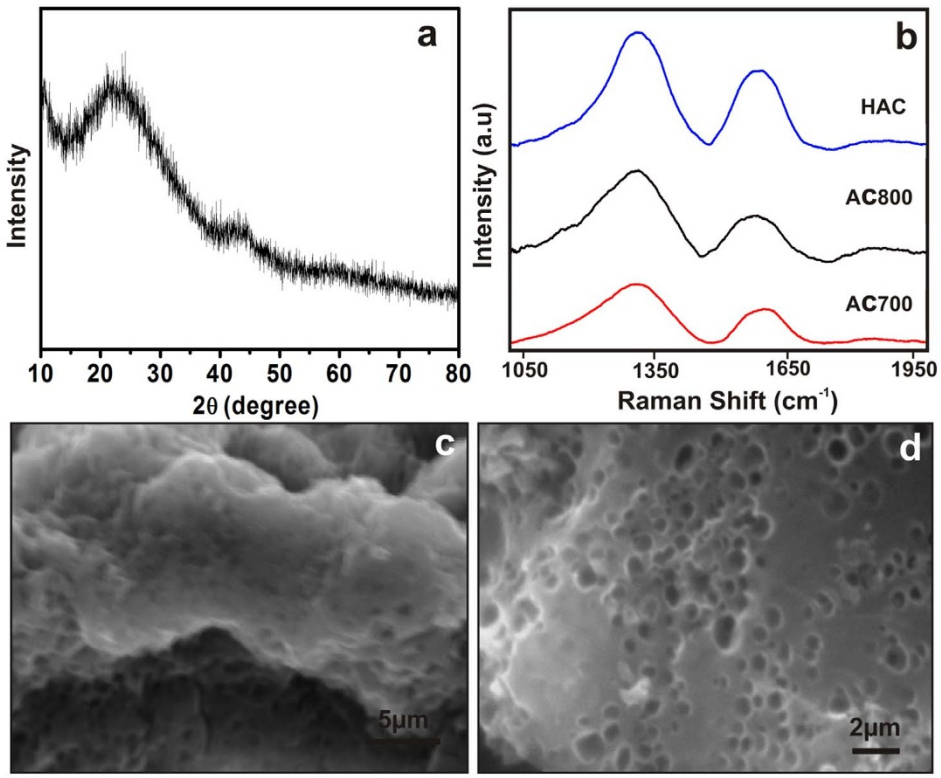

Figure 2 | (a), XRD pattern of HAC. (b), Raman spectra of AC700, AC800 and HAC carbonized samples. (c) and (d), SEM images of the HAC.

tion[41–44]. The peak at 165.4 eV (see Supplementary Figure S2d) denotes the presence of sulfur $2p_{1/2}$. These XPS analyses reveal the presence of heteroatoms such as nitrogen and sulfur atoms in the carbon network in nature. Figure 2c and d show the SEM images of HAC, which clearly indicates a honeycomb-like porous carbon structure, which acts as a channel to allow the easy diffusion of analyte. Furthermore, the FESEM images of the samples of AC700, AC800, HAC, which were obtained by annealing at different temperatures, are shown in Figure 3. Figure 3(a–c) clearly indicates the deficiency of pores at 700°C, and the pore sizes increases when the temperature increases to 800°C, which reveals the reaction between KOH and C (Eq. 1). Similarly, the pores are further developed when the temperature increases to 900°C, most likely because water evaporates from the carbon surface during the activation process. The proposed mechanism is written as follows[45,46]:

$$6KOH + 2C \rightarrow 2K + 3H_2 + 2K_2CO_3 \quad (1)$$

$$K_2CO_3 \rightarrow K_2O + CO_2 \quad (2)$$

$$K_2CO_3 \rightarrow 2C + 2K_2O \quad (3)$$

$$K_2O + C \rightarrow 2K + CO \quad (4)$$

Notably, the KOH activation results in porosity development and an increase in surface area, and another advantage is the creation of –OH surface functional groups on the carbon surface. The –OK groups formed on the carbon surface upon KOH activation, which transformed into –OH groups by ion exchange reaction when the samples were washed with water. Hence, voids can be created when K is removed, which creates a large number of polar functional groups, such as –OH, which makes the carbon surface hydrophilic. In addition, removing K may also create more pores in the samples.

The N_2 adsorption-desorption isotherms and the pore volume of the HAC material are shown in Figure 3d and e. Similar to our previous report, strong N_2 adsorption was observed, which confirms the presence of different pore sizes of micro-, meso- and macropores[12,47]. A surface area of 1465 $m^2\ g^{-1}$ was calculated using the Brunauer-Emmett-Teller (BET) model. The calculated pore volume of HAC was 0.99 $cm^3\ g^{-1}$ using the BJH model. The major advantages of HAC from the banana stem are its large surface area, high-energy adsorption sites (the shapes and size of the isotherms), highly porous nature with high carbon purity, which allows the strong adsorption of the target ions and leads to improved sensitivity[12].

To better understand the electrochemical sensing mechanism, diffusion coefficient, solution resistance and charge transfer resistance at the electrode/electrolyte interfaces, the electrochemical impedance spectroscopy (EIS) analysis is performed. It is well known that the diameter of the semicircle is a direct representation of the charge transfer resistance (R_{ct})[48–51]. Figure 4 represents the Nyquist plots of bare GCE (a), AC700 (b), AC800 (c) and HAC (d) that were studied in 5 mM $Fe(CN)_6^{3-/4-}$ with 0.1 M KCl as the supporting electrolyte. Figure 4 clearly indicates that the bare GCE has higher R_{ct} than the other three modified electrodes, which suggests that the AC samples have lower R_{ct} values. Furthermore, the R_{ct} value decreases with increasing carbonization temperature (AC700, AC800 and

Table 1 | Elemental analysis of AC

Sample (HAC) Weight (mg)	C atom/%	H atom/%	N atom/%	S atom/%
2.028	61.149	2.489	0.438	0.371
1.955	61.092	2.647	0.425	0.328
Mean	**61.12**	**2.567**	**0.4315**	**0.349**

C-Carbon, H-Hydrogen, N-Nitrogen, S-Sulfur.

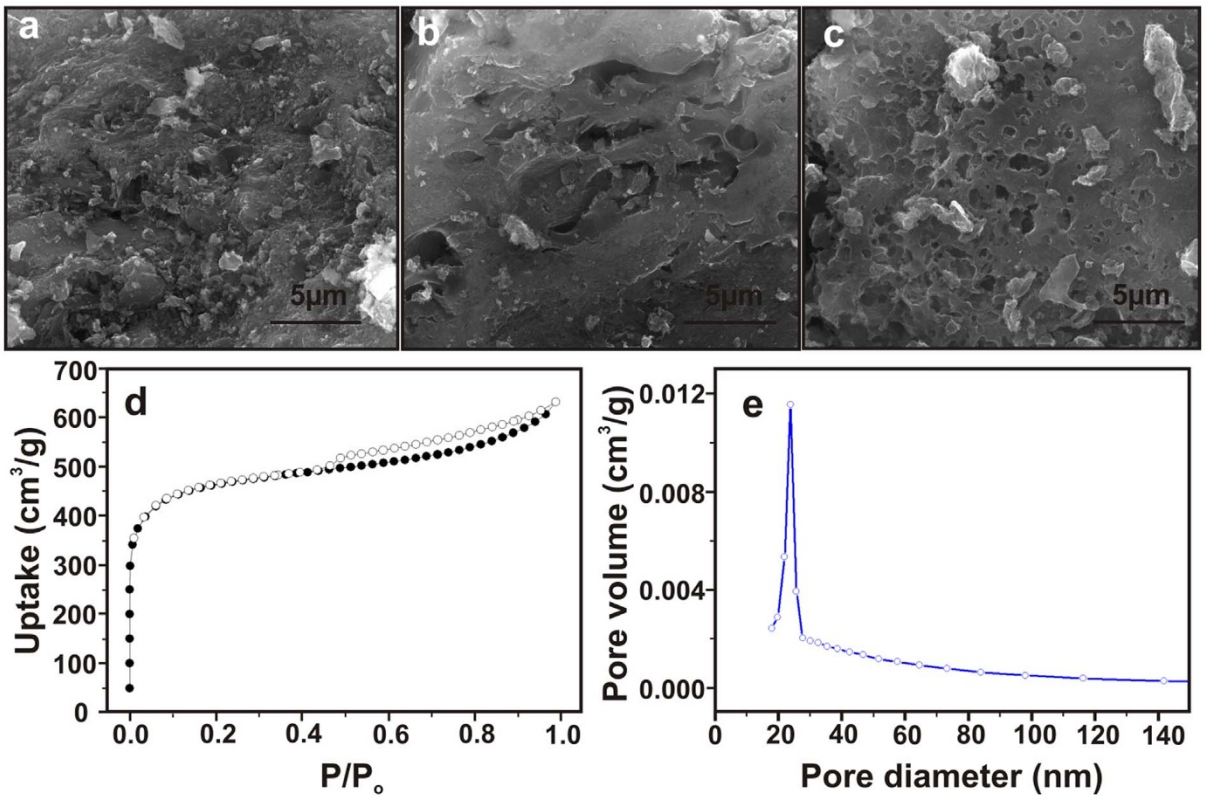

Figure 3 | (a), N_2 adsorption-desorption isotherms. (b), pore diameter vs. pore volume that adsorbed the HAC sample. (a–c) FESEM images of the AC samples at different carbonization temperatures: (c) AC700C, (d) AC800C and (e) HAC.

HAC). Hence, the optimized sample (HAC) was used for electrochemical analysis based on the obtained lower R_{ct} value.

In addition, cyclic voltammetry was used to further characterize the interface properties of the different modified electrodes; the bare GCE (a), AC700 (b), AC800 (c) and AC900 (d) were studied in 5 mM $Fe(CN)_6^{3-/4-}$ with 0.1 M KCl as the supporting electrolyte, as shown in Supplementary Figure S3. Compared with the bare GCE, AC700 gives a well-defined peak and a higher current. For the further modified AC800 and HAC films, the redox peak currents were subsequently increased, which promotes the electron transfer process at the HAC-modified electrode surface compared to the other modified electrodes. The obtained results may occur because there are various oxygen functional groups on the carbon surface of the HAC material. Hence, the creation of heteroatoms while increasing the carbonization temperature (see Supplementary Fig. S2) may provide the necessary conduction pathways on the electrode surface to obtain a better electrocatalytic behavior. This result also reveals that a large number of functional groups are created through KOH activation when the samples are washed with water to remove K. Moreover, the obtained result is consistent with our previous report, which proves the increase in specific capacitance when the carbonization temperature increases[52,12].

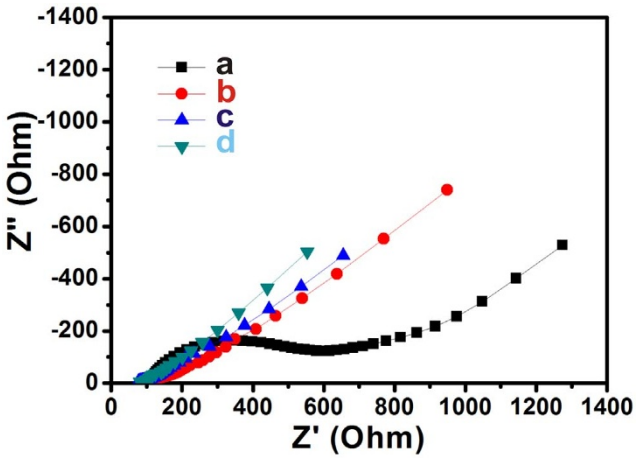

Figure 4 | EIS plots of 5.0 mM $[Fe(CN)6]^{3-/4-}$ in 0.1 M KCl that were recorded at different electrodes of bare (a) AC700 (b), AC800 (c) and HAC (d) modified GCE.

The HAC film exhibits excellent properties when we further optimize the AC at different temperatures for the nitrite sensor. Figure 5 shows the corresponding cyclic voltammogram of different modified electrodes in 50 μM nitrite in a pH 4 PBS buffer solution. In comparison, a similar set of experiments was performed using three different AC-modified GCEs: AC700, AC800 and HAC. Among them, HAC exhibited a large current with a favorable negative potential shift towards the oxidation of nitrite. Interestingly, we chose AC900 for further experiments. The performance of HAC compared with the bare GCE (b) and the blank measurement (c) is shown in the inset of Figure 5 (curve c), which reveals that there is no peak obtained in the absence of analyte. Moreover, the oxidation of NO_2^- for the bare GCE appeared as a broad peak with a peak potential of 1.033 V (curve b), whereas for the HAC-modified GCE (curve a), the peak potential was shifted to 0.7951 V. The favorable negative shift of 237 mV and a 2-fold larger current signal establish that the HAC-modified GCE can greatly facilitate the oxidation of nitrite. The results reveal the excellent properties of HAC such as the presence of heteroatoms, a high specific surface area, a high number of pores and a good electrical conductivity. Moreover, the shape of the isotherms strongly indicates the presence of high-energy adsorption sites, which plays an important role in promoting the electrochemical oxidation of nitrite. Furthermore, these sites attract the

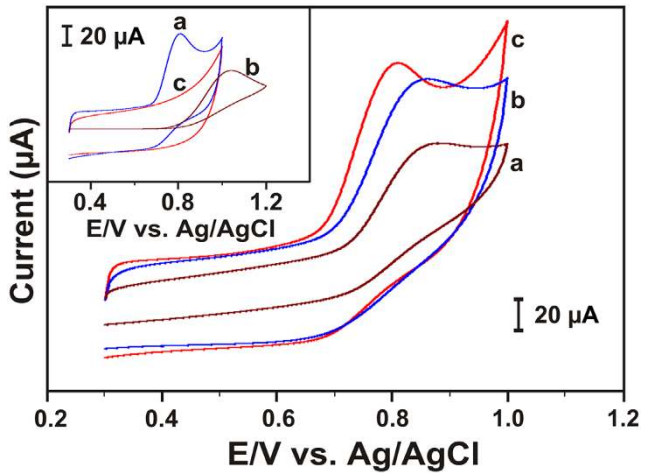

Figure 5 | CVs obtained at AC700 (a), AC800 (b) and HAC (c) modified GCEs in 0.1 M PBS (pH 4), which contained 50 μM nitrite, at the scan rate of 50 mVs^{-1}. Inset: CVs obtained at HAC towards absense (c), presence of nitrite (a) and bare modified GCE (b).

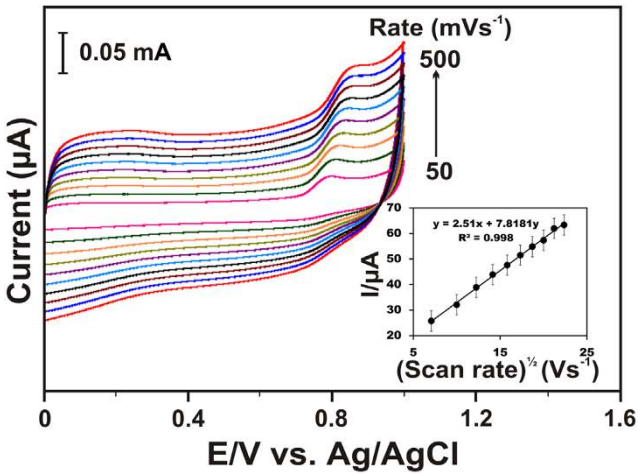

Figure 6 | CVs obtained at HAC-modified GCE at different scan rates in 0.1 M PBS (pH 4), which contained 50 μM nitrite (50-500 mVs^{-1}). Inset: Ip vs. $(\text{scan rate})^{1/2}$ $(Vs^{-1})^{1/2}$, respectively.

negatively charged ions of nirite, and it is possible to accumulate nitrite ions on the electrode surfaces.

Figure 6 shows the corresponding cyclic voltammogram of the HAC-modified electrode with different scan rates in 50 μM nitrite in a pH 4 PBS buffer solution. The voltammogram clearly exhibits that the oxidation peak current (I_{pa}) increases when the scan rates increase, whereas the peak potential positively shifts. Furthermore, the Ipa values also exhibited a linear dependence with the square root of the scan rates (inset) in the range of 50–500 mV s^{-1}. The linear equation is $I_{pa} = 2.51+7.818\ V^{1/2}$ with a correlation coefficient of 0.998. The results suggest that the kinetics of the overall process was controlled by a diffusion process. Moreover, the capacitance also increases with the oxidation peak current, which can be attributed to the pseudocapacitive contribution from the oxygen surface functional groups[53]. These groups can improve the wettability and maximize the electroactive surface area[54].

The HAC-modified electrode has enormous catalytic activity towards the nitrite sensor, possibly because of the heteroatom-enriched nature. The amounts of carbon, hydrogen, nitrogen and sulfur in HAC, which are determined using the CHNS elemental analysis, are 61.12, 2.567, 0.4315, and 0.349%, respectively (see Table 1). The overall reaction is expressed as follows:

$$NO_2^- + H_2O \rightarrow NO_3^- + 2H^+ + 2e^- \quad (5)$$

This process is a second-order homogeneous disproportionation process; NO_3^- is the only oxidation product, which is more preferred for the electrochemical determination of nitrite[55].

Supplementary Figure S4 shows the typical differential pulse voltammetry (DPV) of the electro catalytic oxidation of nitrite at a HAC-modified electrode in different concentrations of nitrite in N_2-saturated PBS. As shown in Supplementary Figure S4, the oxidation peak current of nitrite was observed at 0.767 V, and the peak currents linearly increased with increasing concentrations of nitrite from 3 μM to 90 μM, as shown in Supplementary Figure S3 (inset). The linear equation is $I_p/\mu A = 0.7139\ (\pm 0.072)\ [NO_2^-]/\mu A\mu M^{-1} + 10.972\ (\pm 1.053)$, and $R^2 = 0.9854$. The calculated sensitivity is 9 (± 0.063) $\mu A\mu M^{-1}cm^{-2}$. The calculated lower detection limit (LOD) was 0.13 μM according to the formula LOD = 3 s_b/S (where s_b is the standard deviation of the blank signal, and S is the sensitivity). The results clearly show that the analytical parameters of the reported HAC-modified GCE in this study are superior to those of the other reported materials (see Supplementary Table S1) mainly

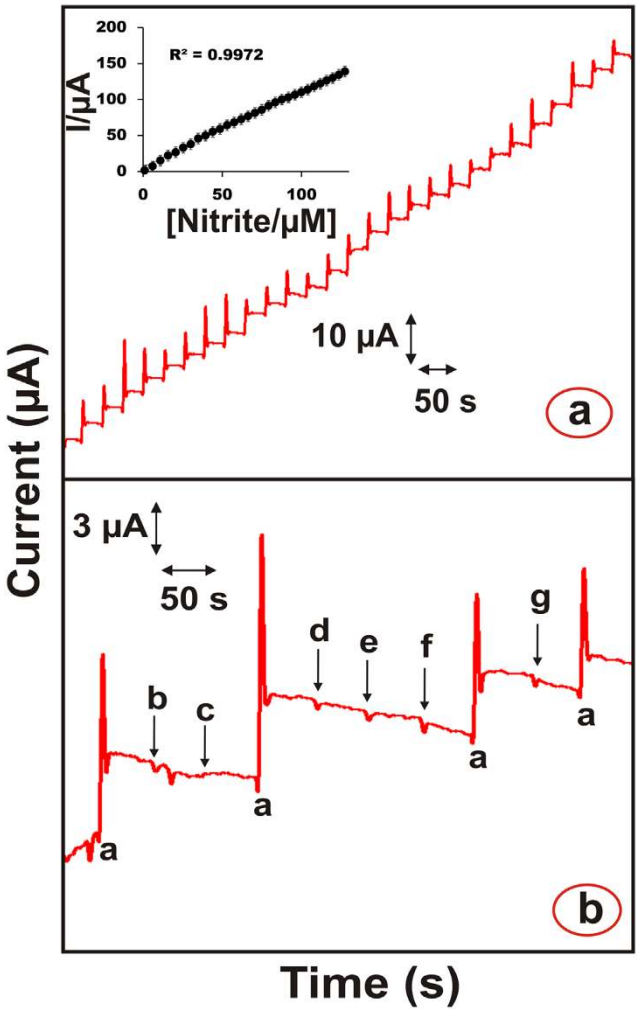

Figure 7 | (a), Amperometric response at the HAC-modified rotating-disc GCE upon successive additions of 1 μM nitrite into a continuously stirred 0.1 M PBS (pH 4) solution. Rotation rate: 1800 rpm; $E_{app} = +0.77$ V. The inset is the corresponding calibration plot of the response current vs. [nitrite]. (b), The amperometric response at the HAC-modified rotating-disc GCE for 25 μM of nitrite(a) in the presence of 1000-fold: urea (b), $NaNO_3$ (c), KCl (d), $ZnCl_2$ (e), $NiCl_2$ (f) and glucose (g).

because of the high-energy adsorption sites of the as-synthesized HAC with high surface area and modulated pore sizes. Hence, the HAC-modified electrode is more suitable for the highly sensitive determination of nitrite sensor.

We also performed the amperometric i-t experiments to obtain better sensitivity and compare with the DPV study. Figure 7a shows the typical amperometric response of HAC-modified electrode with successive addition of 1 μM nitrite in the phosphate buffer solution. The rotation speed of the HAC-modified electrode was 1800 RPM at an applied potential of +0.77 V. The current response is linear with the nitrite concentration in the range 1 μM to 127 μM with the linear equation (inset) of $I_p/\mu A = 1.0548\ (\pm 0.36)\ [NO_2^-]/\mu A\mu M^{-1} + 5.8455\ (\pm 1.14)$ ($R^2 = 0.9972$). The sensitivity is 13 (± 1.26) $\mu A\mu M^{-1}\ cm^{-2}$. The lower detection limit (LOD) was calculated to be 0.07 μM using the formula LOD = $3\ s_b/S$ (where s_b is the standard deviation of the blank signal, and S is the sensitivity). The obtained results for nitrite detection are more comparable than many previously reported carbon- and graphene-based nitrite sensors (see Supplementary Table S1). The result clearly explains that the HAC-modified electrode quickly and sensitively responds to the increase in nitrite concentration. The current response time of the HAC-modified electrode was less than 2 s after the addition of nitrite. The well-defined and fast amperometric response occurs because of the highly porous nature of the HAC material, which acts as a reservoir to reduce the ion diffusion length of the ions from the electrolyte.

The possible interference for the nitrite detection was investigated by adding some inorganic ions and organic compounds, which may coexist with nitrite in real samples, into the pH 4.0 PBS solution. As shown in Figure 7b, HAC/GCE exhibits well defined amperometric response towards each addition of 25 μM nitrite (a). However, there was no significant response observed for each 1000-fold excessive addition of urea (b), $NaNO_3$ (c), KCl (d), $ZnCl_2$ (e), $NiCl_2$ (f) and glucose (g). Interestingly, every addition of nitrite (a) produced a noteworthy response, which reveals excellent selectivity of the proposed sensor. The results clearly demonstrate that nitrite can be selectively detected by HAC/GCE even when there are large quantities of other common species. The storage stability of the proposed sensor was investigated in 50 μM nitrite with pH 4.0 PBS at 4°C, and the oxidation peak current response was periodically monitored. The sensor retains approximately 91.2% of its initial oxidation peak current response after one week, which indicates the good storage stability of the sensor. The 3 independently prepared electrodes to determine 50 μM nitrite show an acceptable reproducibility with an RSD of 3.6%. The repeatability of 10 successive measurements with the RSD of 4.5% to determine 50 μM nitrite indicates a good repeatability of the proposed nitrite sensor. To investigate the possible use of the proposed method, the experiments were studied in various water samples (river, sea and tap water) to determine nitrite by DPV using the standard addition method. The results are shown in Table 2, and the recoveries ranged between 96.0% and 102.4%. Therefore, the developed sensor can be preliminarily applied to determine nitrite in environmental samples.

In summary, we prepared a new carbon material from banana stems *(Musa paradisiaca, Family: Musaceae)* using a simple and eco-friendly method, and a high surface area of approximately 1456 m^2g^{-1} is reported for the first time. The HAC exhibited a significant performance for the determination of the nitrite sensor. In addition, the obtained ultrahigh sensitivity of nitrite is 9 or 13.2 $\mu A\mu M^{-1}cm^{-2}$. The nitrite sensor has high sensitivity and a low detection limit because the HAC has heteroatoms with higher surface area and modulated pore size, where the pores act as reservoirs and reduce the ion diffusion length of the ions from the electrolyte. Furthermore, the proposed method was applied to determine nitrite in various water samples with acceptable results.

Table 2 | Determination of NO_2^- in various real samples using DPV

Real samples	Analyte	Added (μM)	Found (μM)	Recovery (%)
Lake water	NO_2^-	25	24.2	97
		50	50.4	100.8
Sea water	NO_2^-	25	24.8	99.2
		50	51.2	102.4
Tap water	NO_2^-	25	24	96
		50	49.1	98.2

Methods

Materials. Sodium nitrite ($NaNO_2$) was purchased from Sigma-Aldrich. Potassium hydroxide (KOH) was purchased from Shimakyu's Pure Chemicals, Osaka, Japan. Banana stems *(Musa paradisiaca, Family: Musaceae)* were collected from Dharmapuri (Tamilnadu, India). The supporting electrolytes were prepared using 0.1 M of Na_2HPO_4 and NaH_2PO_4, and the pH was adjusted by NaOH or H_2SO_4. All other solutions were prepared using double distilled water.

Instrumentation. The cyclic voltammetry (CV) and differential pulse voltammetry (DPV) studies were performed using a CHI 900 electrochemical analyzer (CH instruments). The elemental analysis was performed using the "elementar Vario EL cube" (for NCSH, German). The surface morphology of the film was studied using JEOL field-emission scanning electron microscopy. X-ray diffraction (XRD) was performed on a Rigaku, MiniFlex II instrument. The Raman spectra were recorded at ambient temperature using a WITeck CRM200 confocal microscopy Raman system with a 488 NM laser. The N_2 adsorption-desorption isotherms and the pore size distribution were studied using "Micromeritics ASAP 2020". The X-ray photoelectron spectroscopy was studied by using XPS, PerkinElmer PHI-5702. A conventional three-electrode cell system was used with a modified glassy carbon electrode (GCE) as the working electrode, an Ag/AgCl (saturated KCl) reference electrode and a platinum wire as the counter electrode.

Synthesis of activated carbon. The banana stems *(Musa paradisiaca, Family: Musaceae)* were thoroughly washed and subsequently dried in an oven at 100°C. The pulverized banana stems were preheated at 200°C for 6 h to remove the moisture. For the activation process, the preferred amount of preheated powder was added to 10% KOH in an N_2 atmosphere while stirring at 60°C. Then, the activated sample was placed in open atmosphere for 24 h. To optimize the activation temperature, 10 g of banana stem powder was heated in a quartz crucible at different temperatures of 700, 800 and 900°C for 2 h in a nitrogen atmosphere at a heating rate of 10°C min^{-1} in a tubular furnace. The carbonized samples were washed with distilled water and 1 M HCl until the pH became neutral. Then, the samples were dried at 100°C overnight to remove moisture and then thoroughly ground to yield the finest powder.

Fabrication of the HAC-modified electrode. The as-prepared, purified AC900°C (HAC) was dispersed in ethanol and sonicated for 2 hours to obtain a stable dispersion. Prior to modification, the GCE surface was carefully polished to a mirror finish with alumina slurry. Then, it was washed with distilled water and ultrasonicated in ethanol-containing water for a few minutes. Approximately 6 μl of HAC dispersion (optimized concentration) was drop-cast on the pre-cleaned GCE and dried in air oven at 30°C. Then, the HAC-modified GCE was gently rinsed a few times with double distilled water to remove the loosely bound HAC. The fabricated HAC-modified electrode was used for further electrochemical experiments, and all the experiments were performed at room temperature in an inert atmosphere.

1. Kruk, M. *et al.* Synthesis of Mesoporous Carbons Using Ordered and Disordered Mesoporous Silica Templates and Polyacrylonitrile as Carbon Precursor. *J. Phys. Chem. B* **109**, 9216–9225 (2005).
2. Ru, A. H. & Zheng, J. T. Study of Microstructure of High-Surface-Area Polyacrylonitrile Activated Carbon Fibers. *J. Colloid Interface Sci.* **236**, 369–374 (2001).
3. Hayashi, J., Kazehaya, A., Muroyama, K. & Watkinson, A. P. Preparation of activated carbon from lignin by chemical activation. *Carbon* **28**, 1873–1878 (2000).
4. Luo, J., Jang, H. D. & Huang, J. Effect of sheet morphology on the scalability of graphene-based ultracapacitors. *ACS Nano* **7**, 1464–1471 (2013).
5. Zhi, M., Xiang, C., Li, J. & Wu, N. Nanostructured carbon-metal oxide composite electrodes for supercapacitors: a review. *Nanoscale* **5**, 72–88 (2013).
6. Sun, L. *et al.* From coconut shell to porous graphene-like nanosheets for high-power supercapacitors. *J. Mater. Chem. A* **1**, 2013, 6462–6470.
7. Vernersson, T., Bonelli, P. R., Cerrella, E. G. & Cukierman, A. L. Arundo donax cane as a precursor for activated carbons preparation by phosphoric acid activation. *Bioresour. Technol.* **83**, 95–104 (2002).

8. Hejazifar, M., Azizian, S., Sarikhani, H., Li, Q. & Zhao, D. Microwave assisted preparation of efficient activated carbon from grapevine rhytidome for the removal of methyl violet from aqueous solution. *J. Anal. Appl. Pyrolysis.* **92**, 258–266 (2011).
9. Dias, J. M., Alvim-Ferraz, M. C. M., Almedia, M. F., Rivera-Utrilla, J. & Sanchez-Polo, M. Waste materials for activated carbon preparation and its use in aqueous – phase treatment: A review. *J. Environ. Manage.* **85**, 833–846 (2007).
10. Patil, B. S. & Kulkarni, K. S. Development of high surface area activated carbon from waste material. *Int. J. Adv. Eng. Res Studies.* **I**, 109–113 (2012).
11. Senthilkumar, S. T., Selvan, R. K., Lee, Y. S. & Melo, J. S. Electric double layer capacitor and its improved specific capacitance using redox additive electrolyte. *J. Mater. Chem. A.* **1**, 1086–1095 (2013).
12. Madhu, R., Vijaya Sankar, K., Chen, S. M. & Selvan, R. K. Eco-friendly synthesis of activated carbon from dead mango leaves for the ultrahigh sensitive detection of toxic heavy metal ions and energy storage applications. *RSC Adv.* **4**, 1225–1233 (2014).
13. Soleimani, M. & Kaghazchi, T. Adsorption of gold ions from industrial wastewater using activated carbon derived from hard shell of apricot stones–An agricultural waste. *Bioresour. Technol.* **99**, 5374–5383 (2008).
14. Sevilla, M. & Fuertes, A. B. Sustainable porous carbons with a superior performance for CO_2 capture. *Energy Environ. Sci.* **4**, 1765–1771 (2011).
15. Sevilla, M., Falco, C., Titiricic, M. M. & Fuertes, A. B. High-performance CO_2 sorbents from algae. *RSC Adv.* **2**, 12792–12797 (2012).
16. Guo, Y. *et al.* The preparation and mechanism studies of rice husk based porous carbon. *Mater. Chem. Phys.* **74**, 320–323 (2002).
17. Kozub, B. R., Rees, N. V. & Compton, R. G. Electrochemical determination of nitrite at a bare glassy carbon electrode; why chemically modify electrodes? *Sensor Actuat. B.* **143**, 539–546 (2010).
18. Lijinsky, W., Conrad, E. & Bogart, R. V. D. Carcinogenic Nitrosamines formed by Drug/Nitrite Interactions. *Nature.* **239**, 165–167 (1972).
19. Mirvish, S. S. Role of N-nitroso compounds (NOC) and N-nitrosation in etiology of gastric, esophageal, nasopharyngeal and bladder cancer and contribution to cancer of known exposures to NOC. *Cancer Lett.* **93**, 17–48 (1995).
20. Zhanga, T., Fan, H. & Jin, Q. Sensitive and selective detection of nitrite ion based on fluorescence superquenching of conjugated polyelectrolyte. *Talanta.* **81**, 95–99 (2010).
21. Tu, X. H., Xiao, B. D., Xiong, J. & Chen, X. D. A simple miniaturised photometrical method for rapid determination of nitrate and nitrite in freshwater. *Talanta.* **82**, 976–983 (2010).
22. Chen, G. H., Yuan, D. X., Huang, Y. M., Zhang, M. & Bergman, M. In-field determination of nanomolar nitrite in seawater using a sequential injection technique combined with solid phase enrichment and colorimetric detection. *Anal. Chim. Acta.* **620**, 82–88 (2008).
23. Zhang, M., Zhang, Z., Yuan, D. X., Feng, S. C. & Liu, B. M. An automatic gas-phase molecular absorption spectrometric system using a UV-LED photodiode based detector for determination of nitrite and total nitrate. *Talanta.* **84**, 443–450 (2011).
24. Lin, C. Y., Balamurugan, A., Lai, Y. H. & Ho, K. C. A novel poly (3,4-ethylenedioxythiophene)/iron phthalocyanine/multi-wall carbon nanotubes nanocomposite with high electrocatalytic activity for nitrite oxidation. *Talanta.* **82**, 1905–911(2010).
25. Li, P. *et al.* Self-Assembly of Tetrakis (3-Trifluoromethylphenoxy)Phthalocyaninato Cobalt(II) on Multiwalled Carbon Nanotubes and Their Amperometric Sensing Application for Nitrite. *ACS Appl. Mater. Interfaces* **5**, 2255–2260 (2013).
26. Zhoua, L., Wanga, J. P., Gaia, L., Li, D. & Li, Y. B. An amperometric sensor based on ionic liquid and carbon nanotube modified composite electrode for the determination of nitrite in milk. *Sensors and Actuators B* **181**, 65–70 (2013).
27. Mani, V., Periasamy, A. P. & Chen, S. M. Highly selective amperometric nitrite sensor based on chemically reduced graphene oxide modified electrode. *Electrochem. Commun.* **17**, 75–78 (2012).
28. Zhanga, D. *et al.* Direct electrodeposion of reduced graphene oxide and dendriticcopper nanoclusters on glassy carbon electrode for electrochemical detection of nitrite. *Electrochim. Acta.* **107**, 656–663 (2013).
29. Cui, L., Pu, T., Liu, Y. & He, X. Layer-by-layer construction of graphene/cobalt phthalocyanine composite film on activated GCE for application as a nitrite sensor. *Electrochim. Acta.* **88**, 559–564 (2013).
30. Li, S. J. *et al.* A sensitive and selective nitrite sensor based on a glassy carbon electrode modified with gold nanoparticles, and sulfonated graphene. *Microchim. Acta.* **180**, 821–827 (2013).
31. Mani, V., Wu, T. Y. & Chen, S. M. Iron nanoparticles decorated graphene-multiwalled carbon nanotubes nanocomposite-modified glassy carbon electrode for the sensitive determination of nitrite. *J Solid State Electrochem.* **18**, 1015–1023 (2014).
32. Li, X. R. *et al.* Synthesis of Potassium-Modified Graphene and Its Application in Nitrite-Selective Sensing. *Adv. Funct. Mater.* **22**, 1981–1988 (2012).
33. Mani, V., Dinesh, B., Chen, S. M. & Saraswathi, R. Direct electrochemistry of myoglobin at reduced graphene oxide-multiwalled carbon nanotubes-platinum nanoparticles nanocomposite and biosensing towards hydrogen peroxide and nitrite. *Biosens. and Bioelectron.* **53**, 420–427 (2014).
34. Ye, D., Luo, L., Ding, Y., Chen, Q. & Liu, X. A novel nitrite sensor based on graphene/polypyrrole/chitosan nanocomposite modified glassy carbon electrode. *Analyst* **136**, 4563–4569 (2011).
35. Afkhami, A., Felehgari, F. S., Madrakian, T. & Ghaedi, H. Surface decoration of multi-walled carbon nanotubes modified carbon paste electrode with gold nanoparticles for electro-oxidation and sensitive determination of nitrite. *Biosensors and Bioelectronics* **51**, 379–385 (2014).
36. Zhanga, Y., Zhao, Y., Yuan, S., Wanga, H. & He, C. Electrocatalysis and detection of nitrite on a reduced graphene/Pd nanocomposite modified glassy carbon electrode. *Sensors and Actuators B* **185**, 602–607 (2013).
37. Lv, Y. *et al.* A self-template synthesis of hierarchical porous carbon foams based on banana peel for supercapacitor electrodes. *J. Power Sources* **209**, 152–157 (2012).
38. Wang, L., Zhang, L. C., Cheng, J. X., Ding, C. X. & Chen, C. H. Watermelon used as a novel carbon source to improve the rate performance of iron oxide electrodes for lithium ion batteries. *Electrochim. Acta.* **102**, 306–311 (2013).
39. Datsyuk, V. *et al.* Chemical oxidation of multiwalled carbon nanotubes. *Carbon.* **46**, 833–840 (2008).
40. Chmiola, J., Largeot, C., Taberna, P. L., Simon, P. & Gogotsi, Y. Monolithic Carbide-Derived Carbon Films for Micro-Supercapacitors. *Science.* **328**, 480 (2010).
41. Zhu, Y. *et al.* Carbon-Based Supercapacitors Produced by Activation of Graphene. *Science.* **332**, 1537–1540 (2011).
42. Maldonado, S. & Stevenson, K. J. Influence of Nitrogen Doping on Oxygen Reduction Electrocatalysis at Carbon Nanofiber Electrodes. *J. Phys. Chem. B* **109**, 4707–4716 (2005).
43. Shen, W., Li, Z. & Liu, Y. Surface Chemical Functional Groups Modification of Porous Carbon. *Recent Patents on Chemical Engineering.* **1**, 27–40 (2008).
44. Huang, Y. *et al.* 'Bridge' effect of CdS nanoparticles in the interface of graphene–polyaniline composites. *J. Mater. Chem.* **22**, 10999–1100 (2012).
45. Qie, L. *et al.* Synthesis of functionalized 3D hierarchical porous carbon for highperformance supercapacitor. *Energy Environ. Sci.* DOI: 10.1039/C3EE41638K (2013).
46. Wang, J. & Kaskel, S. Carbon-Based Supercapacitors Produced by Activation of Graphene. *J. Mater. Chem* **22**, 23710–23725 (2012).
47. Biswal, M., Banerjee, A., Deo, M. & Ogale, S. From dead leaves to high energy density supercapacitors. *Energy Environ. Sci.* **6**, 1249–1259 (2013).
48. Nishikata, A., Ichihara, Y. & Tsuru, T. An application of electrochemical impedance spectroscopy to atmospheric corrosion study. *Corros. Sci.* **37**, 897–911 (1995).
49. Mansfield, F. Electrochemical impedance spectroscopy (EIS) as a new tool for investigating methods of corrosion protection. *Electrochim. Acta* **35**, 1533–1544 (1990).
50. Mohsen, Q., Fadl-allah, S. S. & El-Shenawy, N. S. Electrochemical Impedance Spectroscopy Study of the Adsorption Behavior of Bovine Serum Albumin at Biomimetic Calcium – Phosphate Coating. *Int. J. Electrochem. Sci.* **7**, 4510–4527 (2012).
51. Strašàk, L., Dvořàk, J., Hasoň, S. & Vetterl, V. Electrochemical impedance spectroscopy of polynucleotide adsorption. *Bioelectrochemistry.* **56**, 37–41 (2002).
52. Li, W. *et al.* A Self-Template Strategy for the Synthesis of Mesoporous Carbon Nanofibers as Advanced Supercapacitor Electrodes. *Adv. Energy Mater.* **1**, 382–386 (2011).
53. Hall, P. J. *et al.* Energy storage in electrochemical capacitors: designing functional materials to improve performance. *Ener. Env. Sci.* **3**, 1238–1251 (2010).
54. Wei, Y. *et al.* SnO_2/Reduced Graphene Oxide Nanocomposite for the Simultaneous Electrochemical Detection of Cadmium(II), Lead(II), Copper(II), and Mercury(II): An Interesting Favorable Mutual Interference. *J. Phys. Chem. C* **116**, 1034–1041 (2012).
55. Guidelli, R., Pergola, F. & Raspi, G. Voltammetric Behavior of Nitrite Ion on Platinum in Neutral and Weakly Acidic Media. *Anal. Chem.* **44**, 745–755 (1972).

Acknowledgments

This work was supported by the National Science Council and the Ministry of Education of Taiwan (ROC).

Author contributions

R.M. conceived and synthesized the AC from banana stem. Furthermore, he performed the structural, surface, and morphological analysis and wrote the paper. R.M. and V.V. performed the electrochemical detection of the nitrite experiments. The project was finalised by S.M.C. All authors discussed the results and commented on the manuscript.

Additional information

Supplementary information accompanies this paper at http://www.nature.com/scientificreports

Competing financial interests: The authors declare no competing financial interests.

How to cite this article: Rajesh, M., Veeramani, V. & Chen, S.-M. Heteroatom-enriched and renewable banana-stem-derived porous carbon for the electrochemical determination of nitrite in various water samples. *Sci. Rep.* **4**, 4679; DOI:10.1038/srep04679 (2014).